Length scales relating the fluid permeability and electrical conductivity in random two-dimensional model porous media

N. Martys and E. J. Garboczi
National Institute of Standards and Technology, Building Materials Division, 226/B348, Gaithersburg, Maryland 20878
(Received 16 April 1992)

We present results of a study testing proposed length scales l relating the bulk electrical conductivity σ of a fluid-saturated porous medium to its permeability k, via the relation $k \propto l^2\sigma/\sigma_0$, where σ_0 is the fluid conductivity. For a class of two-dimensional model random porous media, we compute σ, k, and the following three length scales: h, the ratio of pore volume to pore surface area; Λ, as defined by electrical-conductivity measurements; and d_c, as defined by a nonwetting-fluid-injection experiment. Over a range of two and half decades in k, we find that both Λ and d_c are reasonably good predictors of k, whereas h clearly fails. We also examine differences between the electric fields and the fluid-flow fields for a given pore structure by comparing their respective two-point correlation functions. The length scale Λ is analytically related to an electric-field correlation length, and is found, to a good approximation, to be proportional to a fluid-velocity correlation length. The results of this paper demonstrate the important effect that spatial randomness in the pore space has on flow problems. In a random pore structure, with a distribution of pore sizes, the flow will tend to go more through the largest pore necks, decreasing the importance of the narrowest necks that tend to dominate the behavior of periodic models.

I. INTRODUCTION

There are a wide variety of random, porous materials, whose transport properties are of scientific and technological interest.[1,2] Important examples include sedimentary rocks, soils, catalysts, ceramic filters, and cement-based materials such as concrete. Transport properties include the rate of either diffusive, electrical, or fluid movement through fluid-filled pore space. The technological reasons for interest in these transport properties varies from material to material. For example, the rate of flow of water and oil in sedimentary rock is important to the petroleum industry, while the water-aided movement of ions is more important for cement-based materials and plays a central role in their degradation, and in their use as containment barriers for toxic and radioactive wastes. In general, however, a common scientific goal for all such materials is to develop a quantitative understanding of the relationship between pore structure and transport properties.

Recently, there has also been considerable interest[3–9] in relationships *between* transport properties. In particular, the question of the existence of a useful relationship between the fluid permeability k of a fluid-saturated porous material, and its bulk electrical conductivity σ has been studied. The fluid permeability is defined via Darcy's law:[1]

$$v = -\frac{k\,\Delta P}{\eta L}\ , \tag{1}$$

where v is the fluid velocity averaged over the total cross section of the porous sample, η is the fluid viscosity, and ΔP is the pressure drop over the sample length L. The analogous defining equation for the bulk conductivity of the same porous material, where the saturating fluid is a conductor and the solid phase is an insulator, is Ohm's law:

$$\frac{I}{A} = \sigma\frac{\Delta V}{L}\ , \tag{2}$$

where ΔV is the potential drop across a sample of length L and cross-sectional area A, and I is the total current passing through the sample. We define $\Gamma \equiv \sigma/\sigma_0$, where σ_0 is the conductivity of the saturating fluid, as the dimensionless conductivity. Since k has dimensions of length squared, a length scale l, based on the pore structure, must be defined in order to relate k and Γ.

To show heuristically how k and Γ separately depend on pore structure, it is useful to write them as[1,3,4]

$$\Gamma = \beta\phi, \quad k = \beta'\phi l^2\ , \tag{3}$$

where ϕ is the total porosity, which corrects for the reduced cross-sectional area available for flow, l is some length scale defined by the pore structure, and β and β' are factors that take into account pore shape, tortuosity, connectivity, etc. Given Eq. (3), it is easy to see that an estimate of k can be made by using $\Gamma = \beta\phi$ as an estimate of the $\beta'\phi$ product, and then defining a pore structure length scale l. The prediction for k would then be

$$k = c\Gamma l^2\ , \tag{4}$$

where $c = \beta'/\beta$ is an unknown, but hopefully calculable, constant scale factor. Different predictions of the appropriate length scale l have been made in the literature. We consider the three following length scales: h, the pore volume divided by the pore surface area, sometimes called the hydraulic radius;[1] Λ, defined by electrical-conductivity measurements;[3] and d_c, defined by a nonwetting-fluid-injection experiment.[4] A fourth length scale defined in terms of a diffusion-limited trapping

length, which we do not consider, has also been examined[5,6] and shown to have limited success in predicting permeability.

The physical assumptions that underlie the usage of the above-mentioned length scales are quite different. It is therefore important to test and compare each length scale in order to understand what properties of a material's pore structure most strongly determine its permeability. It is also of interest to try to determine how and if, at a fundamental level, the electrical and fluid-flow problems are related. In this paper we carry out this program using computer simulation, applied to a simple two-dimensional (2D) model of a continuum *random* porous material. Such an experimental program has been suggested by Le Doussal,[7] and computer simulation studies with similar goals,[5,8] using mainly periodic models, appeared as this manuscript was in preparation.

An outline of this paper is as follows. In Sec. II the various length scales are defined and in Sec. III we discuss the structural models and algorithms used to compute k, Γ, and the three length scales. In Sec. IV we analyze the example of a simple periodic porous medium, and in Sec. V results on random porous material models are presented. In Sec. VI, correlation functions are used to quantitatively compare and contrast the electrical and fluid problems. Our findings are discussed and summarized in Sec. VII.

II. PORE-STRUCTURE-DEFINED LENGTH SCALES

The pore volume to pore surface area ratio h is the first and simplest length scale of interest. In this paper, h is actually defined by twice the pore area to pore perimeter ratio, or $2V_p/S$. Quantities such as h sometimes go by the name of hydraulic radius.[1] The use of h as a permeability length scale is motivated by the fact that the value of h in 3D for a circular cylindrical tube of radius R and length L is just $2(\pi R^2 L)/(2\pi RL)=R$, which is obviously the length scale that controls the permeability of the tube. In 2D, h is equal to the tube width d. Physical assumptions that underlie the validity of using h to predict permeability include[1] that (1) the variation of pore size is small, and (2) the fluid-flow field is uniform throughout the pore space.

The second length scale that we consider is the Λ parameter,[3] defined in the following way. If a material's pore space is filled by a conducting fluid with conductivity σ_0, and a potential drop is applied, then Λ is defined by the following ratio of integrals:[3]

$$\frac{2}{\Lambda}=\frac{\int |\mathbf{E}|^2 dS}{\int |\mathbf{E}|^2 dV_p} , \tag{5}$$

where $E(\mathbf{r})$ is the magnitude of the electrical field in the pore space, dV_p is a volume element in the pore space, and dS is a surface element on the pore-solid interface. If the electric field were constant everywhere, like that in a circular cylindrical tube when the potential gradient is along the axis of the tube, then $\Lambda=h$. Since in a real porous medium, this would not be the case, Λ can be thought of as a dynamically weighted hydraulic radius,[5] where regions of small electric field, which would probably have small fluid-flow velocities as well, contribute less than high-field regions. In particular, stagnant regions with little or no flow and fully isolated pores would contribute negligibly to Λ. How well pore space regions with low electrical-current-flow rates actually match up to pore space regions with low fluid-flow rates will be studied in Sec. VI.

The third length scale we consider is denoted as d_c, and is defined[4] by a nonwetting-fluid-injection experiment, typically using mercury, which is nonwetting for most porous materials of interest. Mercury is injected into an evacuated sample under hydrostatic pressure, and the additional amount of mercury intruded for each increase in pressure is monitored. The pressure at which the mercury first forms a continuous, percolating path through the sample is defined as the critical pressure P_c. The continuity of the mercury is monitored electrically.[4,9] If the solid phase of the porous material is an insulator, and the pore space is evacuated, then a nonzero bulk conductivity would only be achieved when the mercury percolates. The critical value of pressure P_c is converted into a critical pore size d_c using the Washburn equation:[10]

$$P_c=\frac{4\gamma\cos\theta}{d_c} , \tag{6}$$

where γ is the surface tension of mercury, and θ is the contact angle of mercury on the solid phase of the porous material of interest. Equation (6) assumes a circular cylindrical geometry for pores.[11]

Physically, the length scale d_c can be thought of as the smallest member of a subset of the pore space containing the largest pores that form a continuous pathway through the pore space.[4,9] This is because, as can be seen in Eq. (6), the injected mercury fills the largest pores at the lowest pressures, and then fills progressively smaller pores as the injection pressure is increased.

III. STRUCTURAL MODELS AND ALGORITHMS

A. Structural models

The structural models studied in this paper are all digital image based.[14] A square array of pixels is defined such that each pixel represents either a solid or liquid phase. Assuming all pixels initially represent fluid, solid circular inclusions are introduced by centering a continuum circle on a pixel center, and changing all pixels to solids whose centers fall inside the boundary of the continuum circle.[15] For circles with diameter greater than 15 pixels, the area of the digital circle varies from the area of the generating continuum circle by less than one percent.[15] Figure 1 shows a 41-pixel-diameter circle, centered on the middle of a pixel. Using circles of diameter 41 pixels or larger, we then construct random porous media by randomly depositing[16] many circles on a 1000×1000 unit cell such that no circles overlap. Periodic boundary conditions are maintained by wrapping pixels that would extend outside the unit cell around to the opposite side. Using monosize circles a porosity of

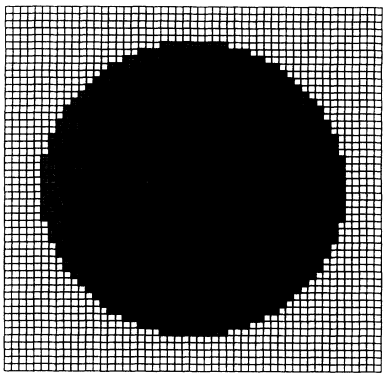

FIG. 1. 41-pixel-diameter digital circle (gray), centered in a 51×51 pixel unit cell.

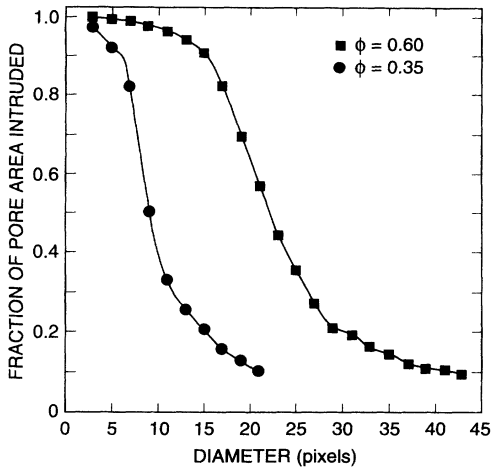

FIG. 2. Two pore-size distributions, computed using the nonwetting-fluid-injection algorithm, and averaged over ten configurations of a 35% and a 60% porosity system of circles deposited in a 1000×1000 pixel unit cell. The curves are normalized by the porosity.

50% can easily be achieved. The lowest porosity achievable for parking of monosize circles is 45%, called the "random jamming limit."[16,17] Lower porosities are attainable using additional, smaller disc sizes. In our case, we tried adding additional disks with a diameter of 21 pixels. However, the spacing between disks at the lower porosities became too small, in terms of numbers of pixels, to ensure adequate resolution and numerical accuracy in the electrical and fluid-flow computations. To be able to explore porosities less than or equal to 50%, we kept the unit cell at 1000×1000 pixels, but "rescaled" the pore space by using 83-pixel-diameter circles as the large-size circle, and 43-pixel-diameter circles as the small-size circle, so that there were fewer circles but more space between circles. Using fewer, larger circles of course meant that our sample statistics became somewhat worse.

B. Nonwetting fluid injection

The algorithm for nonwetting fluid injection has been previously described,[18] and is a geometric method that works only for completely nonwetting fluid injection, in 2D, with a contact angle of 180°. The algorithm begins by surrounding a porous image with a bath of fluid pixels. A pressure is implicitly chosen, via the Washburn equation,[10] by selecting a diameter that is the smallest channel through which the fluid will be allowed to go. The fluid is then successively intruded from the outside by trying to place fluid circles of the chosen diameter, centered at previously intruded fluid pixels. The circular intruding shape gives approximately the correct meniscus, and the chosen diameter guarantees that the fluid will only go into allowed regions. By keeping track of how much pore area was intruded with each choice of the pore diameter, an approximate pore-size distribution can be traced out. Figure 2 shows complete pore-size distributions, averaged over ten realizations of a 60% and a 35% porosity 1000×1000 system. Each curve has been normalized by the total porosity. The value of d_c is determined directly by using a "burning algorithm"[15] to determine when the intruded fluid has percolated. The value of d_c is then the intruding fluid circle diameter at percolation, averaged between the left-right and up-down thresholds, which are not always the same due to finite-size effects.[19]

C. Electrical conductivity and Λ

The dc electrical properties of the model porous media are determined using a finite-difference method of solving Laplace's equation in the pore space. This procedure is equivalent to setting up a random conductor network and solving the Kirchhoff's law network equations.[20] A node is placed in the middle of each pixel, and unit conductance bonds are placed between adjacent pore space pixels. All other nearest-neighbor pairs are assigned zero conductance. Bond assignment is carried out according to periodic boundary conditions. A unit voltage difference is applied in the x direction, and is maintained throughout the conjugate-gradient relaxation process[21] by requiring that nodes separated by the system size L in the x direction differ in voltage by one.

Once the voltage at every node was obtained, the total current was computed to determine the bulk conductivity σ, equal in this case to Γ because σ_0 was normalized to one. The electric fields were computed from the voltages, and used in Eq. (5) to compute Λ directly. We have checked the accuracy of this method against the exact result for a single insulating circle in an $L\times L$ conducting sheet. The relative conductivity for a single isolated circle,[15] with diameter much less than L, is $\Gamma=2\phi-1$, which can be used to show, by using a technique described in Ref. 3 involving adding a very thin conducting layer to the insulating circle, that $\Lambda=L^2/(\pi d)$, where d is the diameter of the circle and ϕ is the porosity. In this limit, h and Λ become equal. Using Eq. (5) with our electric-field results, we found that the computed values of Λ were off by the multiplicative factor $\pi/4$. This is due to the fact that the exact perimeter of a digital circle is $4D$, instead of πD (see Fig. 1), no matter how large the

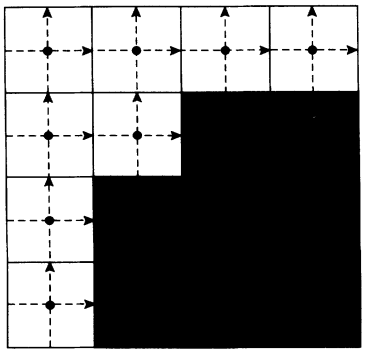

FIG. 3. A piece of a pore space–solid interface. The dark lines are pixel boundaries, and the dashed lines are the superimposed MAC mesh for the fluid-flow computation. The arrows show the locations where the fluid velocities are determined, and the black circles show the nodes where the pressures are determined.

diameter D. The surface integral part of the Λ calculation is then too large. Correcting our Λ results by $4/\pi$ gave the exact results within 2%. All subsequent computations of Λ were corrected by the same factor.

D. Fluid-flow computation

To determine the permeability of our pore structures we numerically solved the Stokes equation[22]

$$\nabla^2\mathbf{v}=\frac{1}{\eta}\nabla P,\quad \nabla\cdot\mathbf{v}=0\ , \tag{7}$$

using a finite difference scheme in conjunction with the artificial compressibility method.[23] The pore space was discretized as a MAC mesh, where MAC stands for "marker-and-cell."[23] A node was centered in each pixel, with pressure defined at the nodes, and velocities defined at the pixel boundaries as shown in Fig. 3. No-slip boundary conditions[22] [$\mathbf{v}(\mathbf{r})=0$] were imposed at all fluid-solid interfaces. In order to improve the accuracy of our solution, noncentered difference equations were used near the pore surface to force the fluid velocities to be zero exactly at pixel boundaries. This results in velocity profiles across channels being accurate to at least second order. A pressure difference was maintained across the microstructure, in the same way that the voltage gradient was maintained in the electrical algorithm. After the fluid velocities were relaxed to their equilibrium values the fluid permeability was determined via Eq. (1). The $\phi=0.35$ models took about 20 min of CPU time for each realization, while the $\phi=0.80$ models took 2–4 h.[24]

IV. TEST OF LENGTH SCALES FOR SIMPLE GEOMETRIES

Certain porous media with simple geometries allow analytical calculations of the quantities studied in this paper. Before results are presented for flow in the more complex random geometries, it is instructive to first examine these simpler cases. These results are summarized in Table I, and discussed below.

For a simple 3D tube with radius R,[22] $k\sim R^2$, h, Λ, and d_c scale as R, and $\Gamma=1$ so that the relation $k=c\Gamma l^2$, with c a contant, holds exactly for all three length scales.

Now consider a periodic square array of insulating solid circular inclusions in two dimensions where L is the spacing between nearest-neighbor circles, d is the circle diameter, $w=L-d$ is the width of the narrowest part of the pore space between the disks, $p=\pi d^2/(4L^2)$ is the inclusion area fraction, and the porosity $\phi=1-p$. We note that ϕ and w are related by $\phi=1-\pi(1-w/L)^2/4$.

We have used exact solutions for this system in various limits as a check of the fluid-flow algorithm, using an $L=301$ pixel square unit cell. In the limit $w\ll L$, a result from lubrication theory[5,25] is that the permeability k is given by

$$k=\frac{2\sqrt{2}}{9\pi}\frac{w^{5/2}}{L^{1/2}}\ , \tag{8}$$

and in the limit $d\ll L$, the permeability is given by[25]

$$k=\frac{L^2}{4\pi}[\ln p^{-1/2}-0.738+p-0.887p^2 +2.038p^3+o(p^4)]\ . \tag{9}$$

Figure 4 shows the computed quantity $\log_{10}(L^2/k)$ plotted vs $p=(1-\phi)$. The solid line is Eq. (8), and the dashed line is Eq. (9). For large values of $1-\phi$ (small values of ϕ), $w\ll L$ and the data points agree well with Eq. (8). The agreement is also still surprisingly good for intermediate values of $1-\phi$, and thus fairly large values of w. The data points at small values of $1-\phi$ ($d\ll L$) agree well with Eq. (9).

Similar "lubrication-theory" calculations can be done for the electrical conductivity,[5] and thus Λ, in the limit $w\to 0$. The technique for calculating Λ using the con-

TABLE I. The relationships between k, Γ, h, Λ, and d_c for a single tube, and for a periodic square array of circles. The tube radius is R, the circle diameter is d, L is the spacing between circle centers, $w=L-d$ is the width of the neck between adjacent circles, and c stands for an arbitrary constant.

	k	Γ	$k/(\Gamma h^2)$	$k/(\Gamma\Lambda^2)$	$k/(\Gamma d_c^2)$
Tube	R^2	1	R	R	R
Periodic circles					
$w\ll L$	$w^{5/2}$	$w^{1/2}$	w^2	c	c
$d\ll L$	$L^2\ln(L/d)$	1	$\ln(L/d)/(L/d)^2$	$\ln(L/d)/(L/d)^2$	$\ln(L/d)$

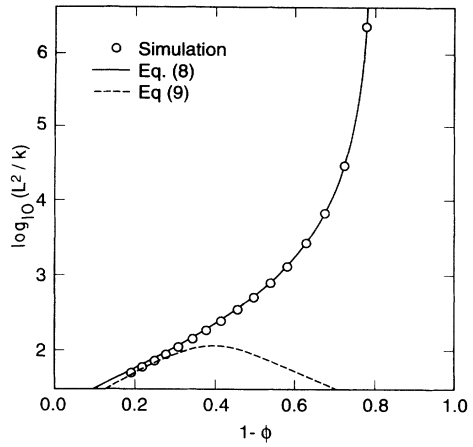

FIG. 4. Permeability k vs porosity ϕ for the periodic square array of circles system. The solid line is Eq. (8) and the dashed line is Eq. (9).

ductivity is taken from Ref. 3. The results are, in the limit $w \to 0$,

$$\frac{\sigma}{\sigma_0} = \frac{\sqrt{2}}{\pi} \left[\frac{w}{L} \right]^{1/2}, \tag{10}$$

$$\Lambda = 2w \ . \tag{11}$$

Figure 5 shows $\Lambda/(2w)$ and $\Gamma = \sigma/\sigma_0$ vs w. The numerical results for conductivity at small w/L do not agree as well with Eq. (10) as the permeability data did with Eq. (8). This is at least partly because the flow of electrical current is not as dominated by the neck as is fluid flow, since the tangential electrical current is not forced to be zero at the edges of the neck like the fluid velocity. This is seen clearly in the differing power laws in w for k and Γ, $\frac{5}{2}$ and $\frac{1}{2}$. Therefore the range of w over which the lubrication theory result holds for the electrical conductivity is much smaller than for the fluid permeability. The numerical results for $\Lambda/(2w)$ are seen to be heading toward the exact asymptotic limit of 1, as $w \to 0$. In the limit $w/L \to 1$, both σ/σ_0 and Λ agree well with the exact asymptotic expressions given in Sec. III, and shown in Fig. 5.

Using the above results, we examine in what regimes the relation $k = c\Gamma l^2$ holds (see Table I). When $w \ll L$, $k \sim w^{5/2}$, $\Gamma \sim w^{1/2}$, and Λ and $d_c \sim w$, so that the relation $k = cl^2\Gamma$ again holds exactly. However, h goes to a constant for $w \ll L$, and hence the relation $k = cl^2\Gamma$ fails for $l = h$. This failure is indicative of h not accurately representing the dynamically connected pore space, as suggested by Johnson, Koplik, and Schwartz.[3] We note that for the case of Λ, $c = \frac{1}{18}$, which is different from the value of $\frac{1}{12}$ that has been proposed for general pore structures.[5] The value of $\frac{1}{12}$ comes from the case of a circular cylindrical tube.[22] In the case where the circle size is small compared with the spacing between circles ($d \ll L$), $k \sim L^2 \ln(L/d)$, $d_c \sim L$, $h \sim L^2/d$, $\Lambda \sim L^2/d$, and all three length scales fail to satisfy the relation $k = c\Gamma l^2$.

V. RESULTS FOR RANDOM SYSTEMS

Figure 6 shows the permeability k (in units of pixels squared) and Fig. 7 shows the relative conductivity Γ for the 1000×1000 pixel unit-cell random systems, plotted vs porosity. For porosities 50% or below, the number ratio of small to large circles was fixed at 1.5. Each data point in Figs. 6 and 7 has been averaged over the x and y directions and over four random structures. The permeability changes by more than two orders of magnitude from $\phi = 0.8$ down to $\phi = 0.35$, with a typical standard deviation computed over the different configurations of about 10% at the higher porosities, increasing to about 30% at the lower porosities. The standard deviation in the conductivity data was never more than a few percent for all porosities.

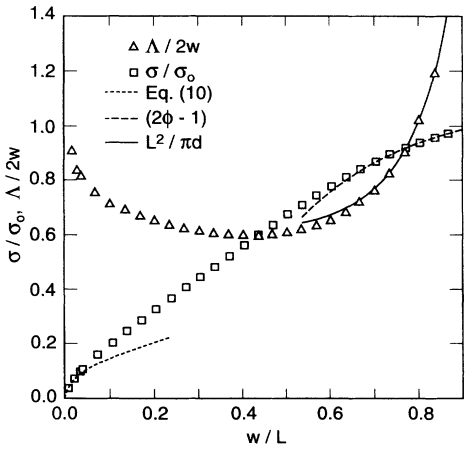

FIG. 5. Quantities $\Lambda/(2d)$ and $\Gamma = \sigma/\sigma_0$ vs the scaled neck width w/L for the periodic square array of circles model. The lines are the exact asymptotic formulas from Eq. (10) (small dashes), $L^2/(\pi d)$ (solid), and $(2\phi - 1)$ (large dashes).

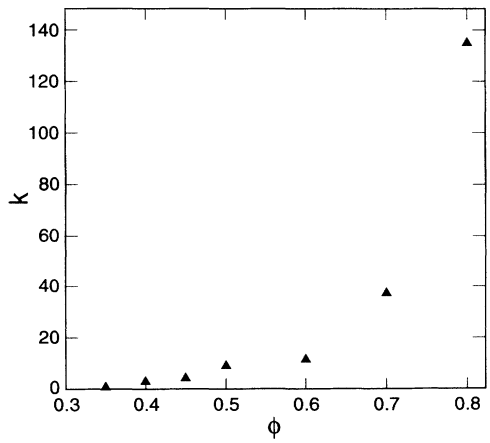

FIG. 6. Permeability k, in units of pixels squared, vs porosity for the 1000×1000 pixel random systems, averaged over the x and y directions and four configurations.

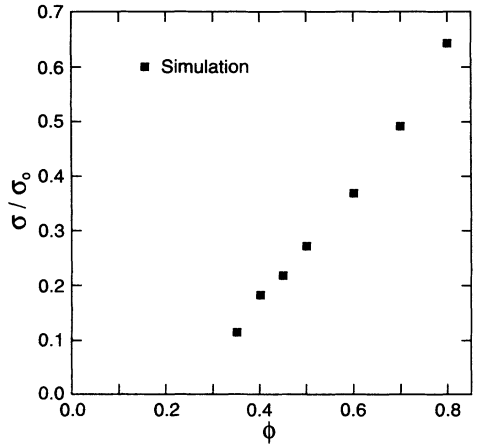

FIG. 7. Showing the relative conductivity $\Gamma=\sigma/\sigma_0$ vs porosity for the 1000×1000 pixel random systems, averaged over the x and y directions and four configurations. The dashed line is the graph of ϕ^2.

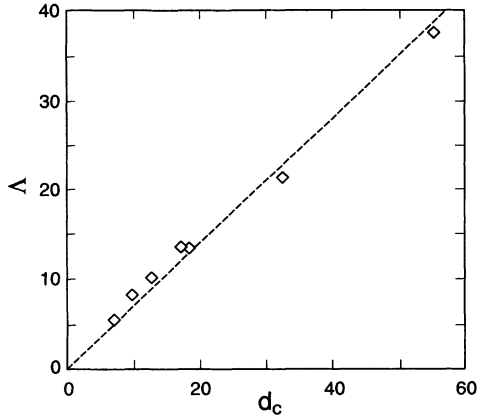

FIG. 9. Λ plotted vs d_c using the data of Fig. 8. The slope of the dashed line is fit to the data, and the line is constrained to go through the origin.

Figure 8 shows the three length scales, Λ, h, and d_c plotted against porosity. Figure 9 shows Λ vs d_c. The Λ-vs-d_c plot in Fig. 9 is roughly linear, in general agreement with the predictions of Banavar and Johnson.[12]

Figure 10 shows the scaled permeabilities for the 1000×1000 pixel unit-cell random models. The permeabilities are scaled by the factor $c'/(\Gamma l^2)$, where the choices of l are (a) $l=\Lambda$, (b) $l=h$, and (c) $l=d_c$, and c' is a constant chosen to make the high-porosity end of each curve be approximately equal to one. Figure 10(a) is quite flat over the whole range of porosity shown, implying that the parameter Λ is giving a good estimate of the pore length scale that is controlling permeability. The value of c' used was 6.5. References 3 and 5 used $c'=1/c=12$ in the relation $k=c\Gamma l^2$.

Figure 10(b), where the permeability is scaled by the hydraulic radius h, with $c'=32$, shows a systematic dip toward lower values as porosity decreases. This is consistent with the results obtained for the periodic-model, since the permeability depends sensitively on the pore necks, while h is determined by all the pore area and volume. Therefore as the critical necks controlling the flow become small while the porosity still remains fairly large, the value of h will increasingly overestimate the permeability length scale.

Figure 10(c) shows how the parameter d_c serves to scale the permeability, with $c'=12$. Reasonably flat behavior is shown across the whole range of porosity, with some rise at lower porosity. The lowest porosity, 0.35, has a significantly narrower pore-size distribution than does the 0.60 porosity system, for example, as can be seen in Fig. 2. Since a basic assumption behind the Katz-Thompson equation is a broad pore-size distribution,[4,9] Fig. 10(c) may be showing a systematic trend in the con-

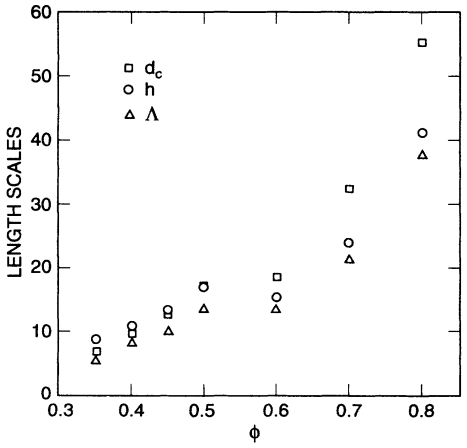

FIG. 8. Three length scales Λ, h, and d_c plotted vs porosity for the 1000×1000 pixel random systems. Each point represents an average over four configurations, and for Λ and d_c, an additional average over the x and y directions.

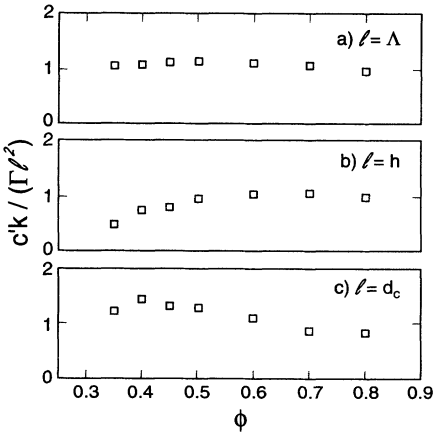

FIG. 10. Permeabilities of Fig. 6, scaled by the values of Γ from Fig. 7 and the length scales of Fig. 8, plotted vs porosity. A different value of c' was used in each graph, in order to make the high-porosity data points fall on the $y=1$ line: (a) $c'=6.5$, (b) $c'=32$, (c) $c'=12$.

stant c' as the pore-size distribution becomes narrower. The constant c' is expected to get smaller for narrower pore-size distributions,[26] which is consistent with our data.

VI. COMPARISON BETWEEN ELECTRICAL AND FLUID-FLOW PROBLEMS

We have verified in Sec. V, in the case of the parameter Λ, that the electrical properties of fluid-saturated porous media can be utilized to give a fairly accurate prediction of its permeability. In this section we study the actual electrical fields and fluid velocity flow fields more closely, and compare then qualitatively, with gray scale pictures, and quantitatively, with correlation functions.

Using the magnitude $v(\mathbf{r})$ of the solution $\mathbf{v}(\mathbf{r})$ to the Stokes equations for a given pore structure, we define the scaled two-point fluid velocity correlation function $S_v(r)$ as the angular average of $S_v(\mathbf{r})$:

$$S_v(r)\equiv\frac{1}{2\pi}\int d\Omega_r S_v(\mathbf{r}) ,$$
$$S_v(\mathbf{r})=\frac{\langle v(\mathbf{r}')v(\mathbf{r}'+\mathbf{r})\rangle_V}{\langle v(\mathbf{r}')v(\mathbf{r}')\rangle_{\text{pore}}} , \tag{12}$$

where the quantity $\langle a(\mathbf{r}')b(\mathbf{r}+\mathbf{r}')\rangle_Q$ is defined by

$$\langle a(\mathbf{r}')b(\mathbf{r}'+\mathbf{r})\rangle_Q=\frac{1}{Q}\int_Q d^2r'[a(\mathbf{r}')b(\mathbf{r}+\mathbf{r}')] , \tag{13}$$

and Q also denotes the area of the region Q. In Eq. (12), the numerator is an integral over the total sample volume V, with $v(\mathbf{r})\equiv 0$ in the solid regions, while the denominator is an integral over the pore space volume V_p only. For an isotropic system, $S_v(\mathbf{r})=S_v(r)$. In our case, the applied pressure gradient breaks the isotropy, so we average over all possible directions of $\mathbf{r}$ to get back a correlation function that depends only on the magnitude of $\mathbf{r}$.

The normalization in Eq. (12) was chosen so that $S_v(0)=V_p/V=\phi$, the porosity. In the limit $r\to\infty$, the fluid velocities must become completely uncorrelated in a pore structure with only short-range structural correlations, so that $S_v(r)$ asymptotically goes to

$$[\langle v(\mathbf{r})\rangle_v]^2/\langle[v(\mathbf{r})]^2\rangle_{\text{pore}}\leq\phi^2 ,$$

and only takes on the equality in the special (unphysical) case when $v(\mathbf{r})=$const everywhere in the pore space. In that special case, the correlation function $S_v(r)$ is actually identical to the two-point correlation function $S(r)$ of the pore structure,[27] where $S(r)=\langle f(r')f(r'+r)\rangle_V$, and the function $f(r')$ is one for pore space and zero for the solid phase. In the more general case of $v(\mathbf{r})\neq$const, we define $S_v(r\to\infty)\equiv\phi_v^2$, where ϕ_v is an effective porosity that measures the part of the total pore space that plays a role in fluid flow. This definition implies that the inequality $\phi_v<\phi$ must strictly hold.

We define the correlation function $S_E(r)$ similarly to $S_v(r)$ in Eq. (12), but with the magnitude of the fluid velocities replaced by the magnitude of the electric fields. Using the method of Ref. 27, it is then straightforward to show that $dS_E(r)/dr=-\phi/(\pi\Lambda)$ at $r=0$, so that the initial slope of this correlation function gives another way to measure Λ. The $r\to\infty$ limit of $S_E(r)$ defines ϕ_E^2, the effective electrical porosity. Also, the initial slope for $S(r)$, the pore space correlation function,[27] is $-2\phi/(\pi h)$ in 2D. The quantities h and Λ can then be considered to be length scales defined by their respective correlation functions. However, using the method of Ref. 27, which turns the numerator of Eq. (12) into a surface integral, it can be shown that $dS_v(r)/dr=0$ at $r=0$, a result that is a direct consequence of the no-slip boundary conditions forcing $\mathbf{v}(\mathbf{r})=\mathbf{0}$ at the fluid-solid interface. We therefore define a length scale L_v from the small-r behavior of this correlation function in a different way, by expanding S_v to second order around $r=0$: $S_v(r)=\phi-\phi(r/L_v)^2$.

Figure 11 plots the three correlation functions $S(r)$, $S_E(r)$, and $S_v(r)$, vs spatial separation r, for an 80% porosity system. The straight dashed lines in Figs. 11(a) and 11(b) are drawn using slopes calculated from direct numerical determinations of h and Λ, while the parabolic dashed line in Fig. 11(c) was fit to the small-r data. Good agreement with the simulation data is seen in all three cases, confirming the above initial slope derivations. The square root of the large-r limit of the correlation functions gives $\phi=0.8$, $\phi_E=0.77$, and $\phi_v=0.62$. The fact that ϕ_E and ϕ_v are both less than ϕ indicates that even at this high porosity, there are areas of the pore space that carry relatively little flow. Furthermore, the inequality $\phi_v<\phi_E$ indicates that there are more of these stagnant areas (with little or no flow) for fluid flow than for electrical current flow.

Figure 12(a) shows a gray-scale image of the electric-

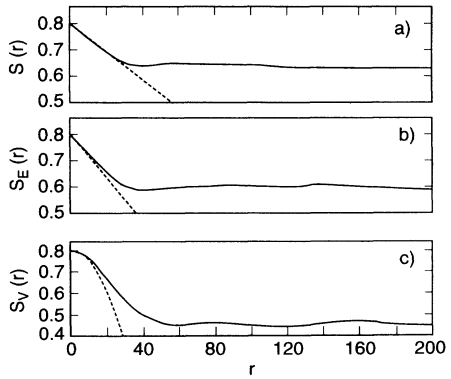

FIG. 11. (a) Pore space, (b) electrical field magnitude, and (c) fluid velocity magnitude correlation functions as a function of distance r, for porosity=0.8. The correlation functions are defined in the text. The dashed lines indicate the exact small-r behavior, defined in the text.

field magnitudes and Fig. 12(b) shows the fluid velocity magnitudes, for an 80% porosity system, where white is the minimum and black is the maximum magnitude of the field quantity being considered. The fluid-flow paths are clearly more concentrated, and follow a more tortuous path than do the electric current paths. It is plain to see that there are significantly more stagnant areas for fluid flow than for electrical current flow.

Figures 13 and 14 are the equivalent of Figs. 11 and 12, but for $\phi=0.5$, and Figs. 15 and 16 show the same results for $\phi=0.35$. As the porosity decreases, the differences between the spatial arrangement of the fluid- and electrical-current-flow fields appear to become more pronounced. The fluid-flow field for $\phi=0.35$, shown in Fig. 16(b), is particularly striking, as one or two main pathways seem to carry almost all the flow. This can be attributed to the flow becoming increasingly controlled by narrow necks, so that the fluid picks out a continuous

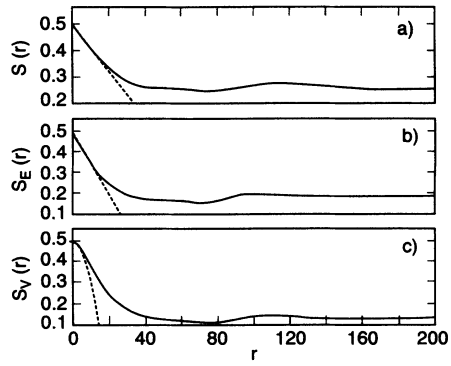

FIG. 13. (a) Pore space, (b) electrical-field magnitude, and (c) fluid velocity magnitude correlation functions as a function of distance r, for porosity=0.5. The correlation functions are defined in the text. The dashed lines indicate the exact small-r behavior, defined in the text.

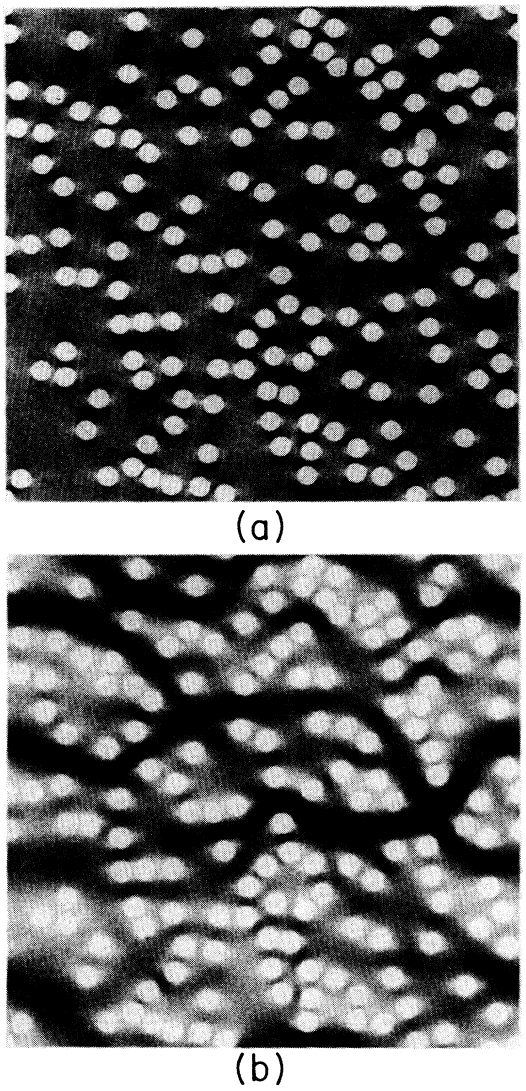

FIG. 12. Gray-scale image of (a) the electric-field magnitudes, and (b) the fluid velocity magnitudes for a porosity of 0.8. White is zero; black is maximum.

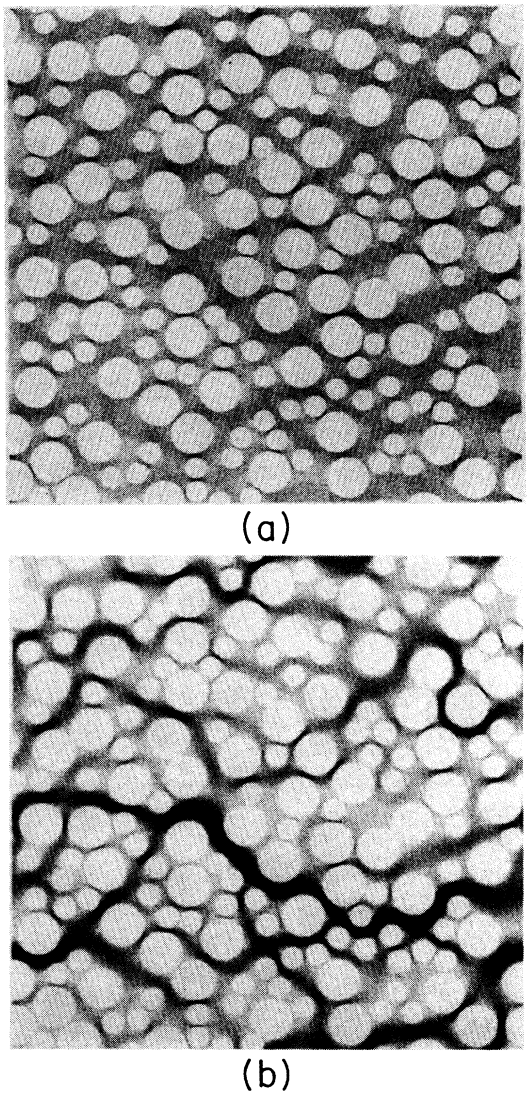

FIG. 14. Gray-scale image of (a) the electric-field magnitudes, and (b) the fluid velocity magnitudes for a porosity of 0.5. White is zero; black is maximum.

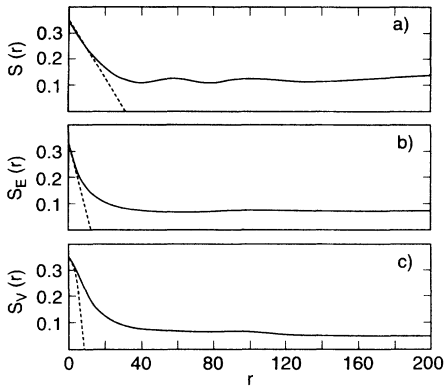

FIG. 15. (a) Pore space, (b) electrical-field magnitude, and (c) fluid velocity magnitude correlation functions as a function of distance r, for porosity=0.35. The correlation functions are defined in the text. The dashed lines indicate the exact small-r behavior, defined in the text.

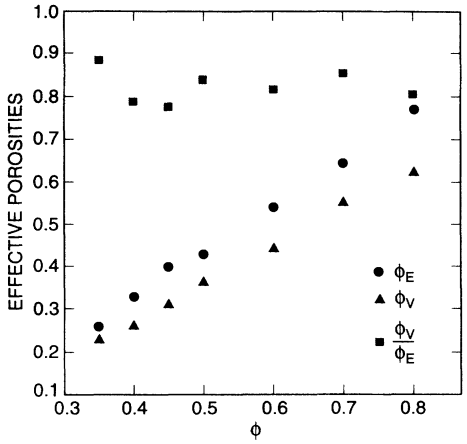

FIG. 17. Electrical and fluid-defined effective porosities ϕ_E and ϕ_v, and their ratio ϕ_v/ϕ_E, plotted against porosity ϕ.

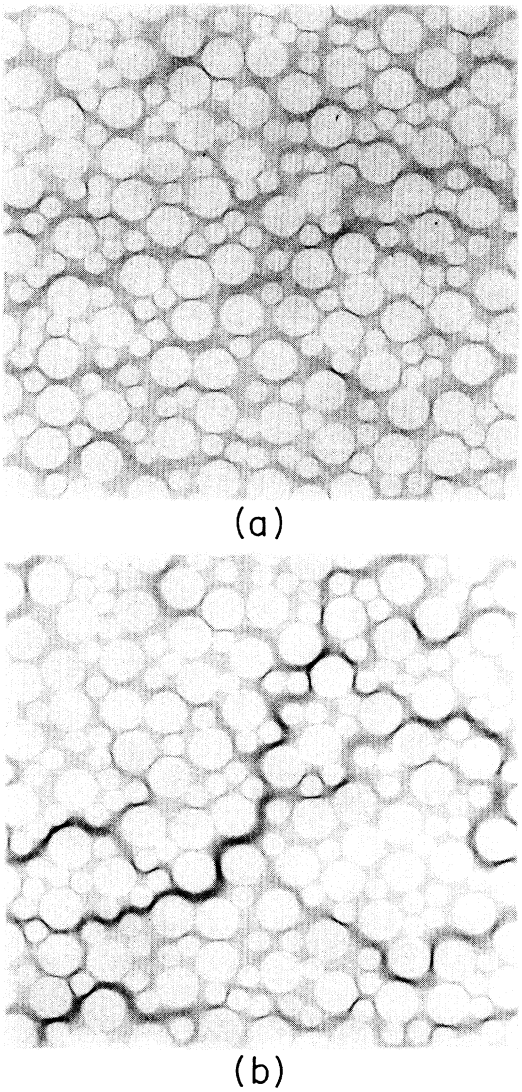

FIG. 16. Gray-scale image of (a) the electric-field magnitudes, and (b) the fluid velocity magnitudes for a porosity of 0.35. White is zero, black is maximum.

path connected by the largest neck sizes. The periodic model from Sec. IV showed how much more sensitive fluid-flow rate is to the width of narrow necks than is the electrical-current-flow rate, due mainly to the no-slip boundary condition.

Figure 17 shows a plot of ϕ_E, ϕ_v, and ϕ_v/ϕ_E, vs ϕ. While the inequality $\phi_v < \phi_E$ holds for all ϕ, the ratio ϕ_v/ϕ_E, surprisingly, remains fairly constant. The sizes of the dynamically connected pore regions are therefore not exactly the same for the electric and fluid-flow cases, but they do decrease in a commensurate fashion with porosity for the model pore structures studied.

Figure 18 shows a plot of L_v vs the length scale Λ. It should be recalled that L_v is extracted from the small-r portion of the fluid velocity correlation function, and Λ is extracted from the small-r portion of the electric-field correlation function. We have found the surprising result, displayed in Fig. 18, that these two length scales are roughly proportional to each other for the model porous

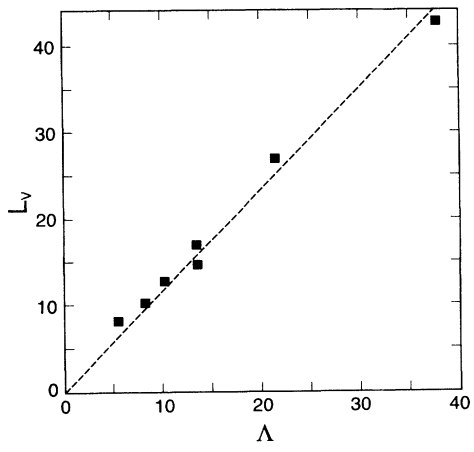

FIG. 18. Fluid velocity length scale L_v plotted against the electrical length scale Λ. The slope of the dashed line is fit to the data, and the line is constrained to go through the origin.

media studied. This is direct quantitative support for the result of Fig. 10(c), which showed that Λ worked well as a length scale to predict permeability. Figure 18 shows that in some sense, the electric fields sample the *local* neighborhood of the important pore necks in a way similar to that of a moving fluid, since L_v and Λ are determined by the small-r behavior of $S_v(r)$ and $S_E(r)$, respectively.

VII. DISCUSSION AND SUMMARY

The utility of using electrical measurements to measure fluid permeability is unquestionable, as electrical measurements are usually easier and faster to make, as long as the value of σ_0 can be readily determined. For sedimentary rocks, the pore fluid is injected, so σ_0 is predetermined, while for cement-based materials, for example, the conductivity of the pore fluid is determined by hydration chemistry[28] and is not so easily determined.

The question that this and other recent papers have focused on is the validity of the basic concept of relating electrical conductivities and fluid permeability quantities. The principal contribution of the present work is that all relevant quantities have been computed on a truly random continuum system, with a reasonably large range of pore sizes. In Ref. 5, the 2D tortuous model considered was constructed such that all pore channels had roughly the same size, so that the electrical-current- and fluid-flow fields looked qualitatively similar. This is a special case. When there is a size distribution of necks through which the flow must go, as is typical in most real porous materials, then, as was shown in Sec. VI the fluid velocity fields and the electric fields can sample the pore space quite differently. The results of this paper demonstrate the important effect that spatial randomness in the pore space has on the two different flow problems. The periodicity of the models considered in Refs. 5 and 8 forces the flow to be one-dimensional, so that all the flow must go through the narrowest neck. However, in a random pore structure, with a distribution of neck sizes, the flow will tend to go more through the largest necks, decreasing the importance of the narrowest necks.

In summary then, we have computed, for a 2D continuum random porous system with a reasonably wide pore size distribution, the permeability k, the electrical conductivity σ, and three pore-space-based length scales Λ, h, and d_c. We have shown that for over two decades in permeability, both Λ and d_c, in conjunction with the electrical conductivity, gave reasonably constant scaling of the permeability. Study of the fluid velocity and electric-current-flow fields via gray-scale images revealed significant qualitative differences between the two kinds of flow. However, a constant ratio between the effective porosities dynamically sampled by the electric and fluid-flow fields, as well as the proportionality between length scales derived separately from two-point electric-field (Λ) and fluid velocity (L_v) correlation functions, lend support to the idea that there may be a deeper connection between the two problems. As to the nature of this connection, we believe that further progress in this area requires more intense theoretical analysis of the basic equations of electrical and fluid flow in a porous medium, similar to work carried out recently by Torquato.[6]

ACKNOWLEDGMENTS

We are grateful for useful discussions with J. R. Banavar, A. Sangani, J. Koplik, S. Kostek, L. M. Schwartz, D. L. Johnson, and A. H. Thompson. The authors would also like to thank D. P. Bentz and W. C. Carter for their assistance in generating the gray-scale images presented in this paper, and P. M. Duxbury for supplying a 2D electrical conjugate-gradient relaxation routine.

[1]A. E. Scheidegger, *The Physics of Flow Through Porous Media* (University of Toronto Press, Toronto, 1974), Chap. 4.
[2]Pozen Wong, Phys. Today **41**(12), 24 (1988).
[3]D. L. Johnson, J. Koplik, and L. M. Schwartz, Phys. Rev. Lett. **57**, 2564 (1986).
[4]A. J. Katz and A. H. Thompson, Phys. Rev. B **34**, 8179 (1986); J. Geophys. Res. **92**, 599 (1987).
[5]S. Kostek, L. M. Schwartz, and D. L. Johnson, Phys. Rev. B **45**, 186 (1992).
[6]S. Torquato, Phys. Rev. Lett. **64**, 2644 (1990); M. Avellaneda and S. Torquato, Phys. Fluids A **3**, 2529 (1991).
[7]P. Le Doussal, Phys. Rev. B **39**, 4816 (1989).
[8]R. B. Saeger, L. E. Scriven, and H. T. Davis, Phys. Rev. A **44**, 5087 (1991).
[9]A. H. Thompson, A. J. Katz, and C. E. Krohn, Adv. Phys. **36**, 625 (1987).
[10]E. W. Washburn, Proc. Natl. Acad. Sci. U.S.A. **7**, 115 (1921).
[11]This assumption has been criticized (Refs. 7 and 12). Recently, this criticism has been addressed by showing that the Katz-Thompson assumption of circular geometry does not automatically preclude accurate predictions of permeability (Ref. 13), as the pore diameter appearing in the Washburn equation is only an effective tube diameter, which integrates over real pore shapes. Reference 13 showed that, at least for elliptical-cross-section tubes, the permeability of the circular tube with the mercury-defined effective diameter was almost identical with the true permeability of the original tube.
[12]J. R. Banavar and D. L. Johnson, Phys. Rev. B **35**, 7283 (1987).
[13]E. J. Garboczi, Powder Technol. **67**, 121 (1991).
[14]K. R. Castleman, *Digital Image Processing* (Prentice-Hall, Englewood Cliffs, 1981).
[15]E. J. Garboczi, M. F. Thorpe, M. DeVries, and A. R. Day, Phys. Rev. A **43**, 6473 (1991).
[16]D. W. Cooper, Phys. Rev. A **38**, 522 (1988).
[17]B. J. Brosilow, R. M. Ziff, and R. D. Vigil, Phys. Rev. A **43**, 631 (1991).
[18]E. J. Garboczi and D. P. Bentz, Ceram. Trans. **16**, 365 (1991).

[19]Fumiko Yonezawa, Shoichi Sakamoto, and Motoo Hori, Phys. Rev. B **40**, 636 (1989).
[20]S. Kirkpatrick, Rev. Mod. Phys. **45**, 574 (1973).
[21]W. H. Press, B. P. Flannery, S. A. Teukolsky, and W. T. Vetterling, *Numerical Recipes: The Art of Scientific Computing (FORTRAN Version)* (Cambridge University Press, Cambridge, 1989).
[22]L. D. Landau and E. M. Lifshitz, *Fluid Mechanics* (Pergamon, London, 1959).
[23]Roger Peyret and Thomas D. Taylor, *Computational Methods for Fluid Flow* (Springer-Verlag, New York, 1983).
[24]Total CPU time used to obtain all results presented in this paper was about 80 h on a two-processor Cray-Research YMP computer, with 16 million words of core memory.
[25]A. S. Sangani and A. Acrivos, Int. J. Multiphase Flow **8**, 193 (1982).
[26]A. H. Thompson (private communication).
[27]J. G. Berryman and S. C. Blair, J. Appl. Phys. **60**, 1930 (1986).
[28]B. J. Christensen, T. O. Mason, and H. M. Jennings, J. Am. Ceram. Soc. **75**, 939 (1992).

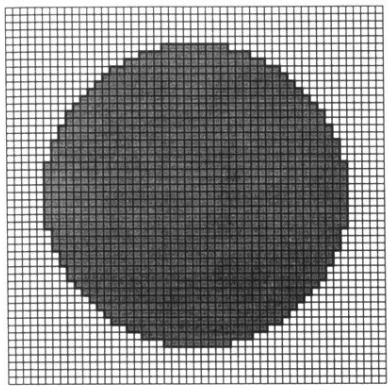

FIG. 1. 41-pixel-diameter digital circle (gray), centered in a 51×51 pixel unit cell.

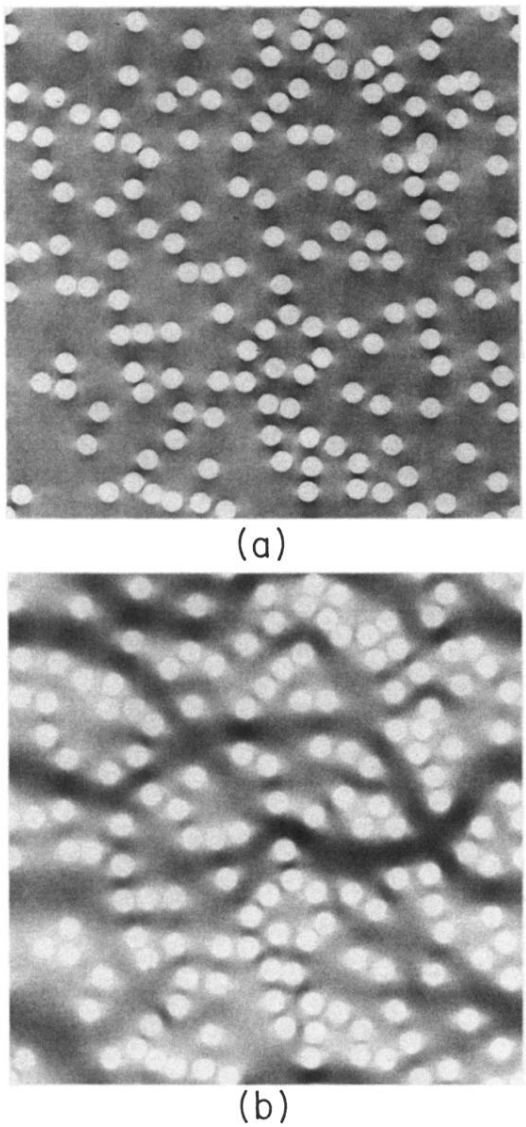

FIG. 12. Gray-scale image of (a) the electric-field magnitudes, and (b) the fluid velocity magnitudes for a porosity of 0.8. White is zero; black is maximum.

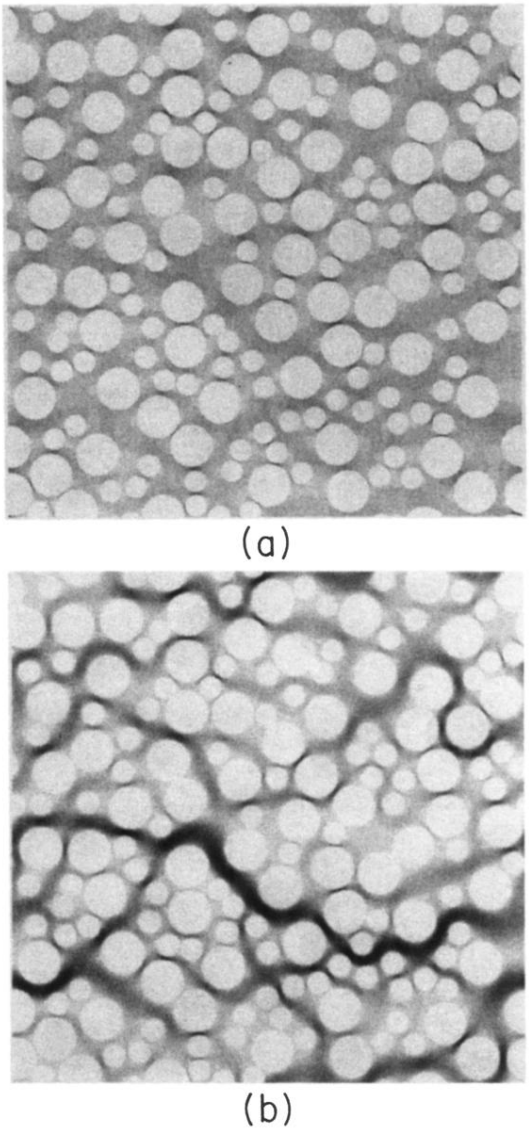

FIG. 14. Gray-scale image of (a) the electric-field magnitudes, and (b) the fluid velocity magnitudes for a porosity of 0.5. White is zero; black is maximum.

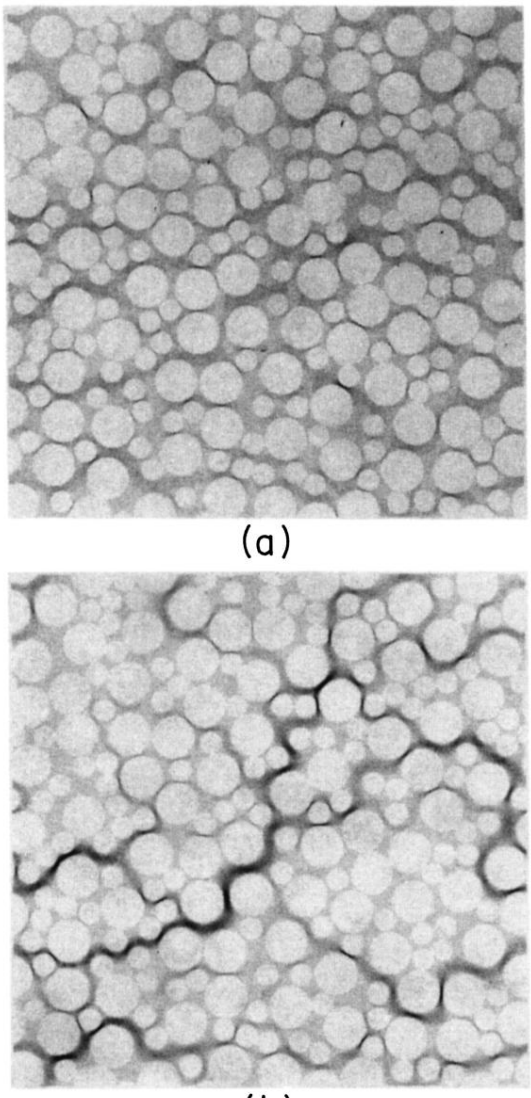

FIG. 16. Gray-scale image of (a) the electric-field magnitudes, and (b) the fluid velocity magnitudes for a porosity of 0.35. White is zero, black is maximum.

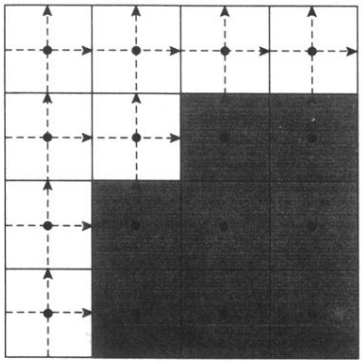

FIG. 3. A piece of a pore space–solid interface. The dark lines are pixel boundaries, and the dashed lines are the superimposed MAC mesh for the fluid-flow computation. The arrows show the locations where the fluid velocities are determined, and the black circles show the nodes where the pressures are determined.